MID-AMERICA TRANSPORTATION CENTER

Report # MATC-MS&T: 133-5

Final Report

WBS: 25-1121-0005-133-5

Over-Height Vehicle Impact with Bridge Girders Having Different Boundary Conditions

Mohamed ElGawady, PhD
Benavides Professor
Department of Civil, Architectural, and Environmental Engineering
Missouri University of Science and Technology

Mohanad Abdulazeez, PhD
Postdoctoral Fellow
Center for Infrastructure Engineering

2024

A Cooperative Research Project sponsored by U.S. Department of Transportation- Office of the Assistant Secretary for Research and Technology

Over-Height Vehicle Impact with Bridge Girders Having Different Boundary Conditions

Mohamed ElGawady, Ph.D.
Benavides Professor
Civil, Architectural and Environmental
Engineering (CArEE)
Missouri University S&T

Mohanad Abdulazeez, Ph.D.
Postdoctoral Fellow
Center for Infrastructure Engineering
Studies (CIES)
Missouri University S&T

A Report on Research Sponsored by

Mid-America Transportation Center

University of Nebraska-Lincoln

September 2024

Technical Report Documentation Page

1. Report No. 25-1121-0005-133-5	2. Government Accession No.	3. Recipient's Catalog No.
4. Title and Subtitle Over-Height Vehicle Impact with Bridge Girders Having Different Boundary Conditions		5. Report Date September 2024
		6. Performing Organization Code
7. Author(s) Mohamed ElGawady, Ph.D., https://orcid.org/0000-0001-6928-9875 Mohanad Abdulazeez, Ph.D., https://orcid.org/0000-0003-4641-9803		8. Performing Organization Report No. 25-1121-0005-133-5
9. Performing Organization Name and Address Missouri University of Science and Technology 300 W 13th St Rolla, MO 65409		10. Work Unit No. (TRAIS)
		11. Contract or Grant No. 69A3551747107
12. Sponsoring Agency Name and Address Office of the Assistant Secretary for Research and Technology 1200 New Jersey Ave., SE Washington, D.C. 20590 Mid-America Transportation Center 2200 Vine St. PO Box 830851 Lincoln, NE 68583-0851		13. Type of Report and Period Covered January 2022-June 2024
		14. Sponsoring Agency Code MATC TRB RiP No. 91994-111
15. Supplementary Notes		

16. Abstract
In recent decades, there has been an increase in catastrophic vehicle-bridge collisions worldwide due to rapid infrastructure development and increased traffic. This study, which addresses the critical research gap in understanding lateral impact loads on prestressed flanged concrete bridge girders, has the potential to impact the field significantly. The paper experimentally investigates the effect of concrete decks as a restraining condition on two small-scale (20 ft long) prestressed girders: Isolated and T-shaped. Using a controlled impact load setup, these girders were subjected to lateral impacts with varying bending and torsional constraints. The test facility simulated over-height vehicle collisions using a 660 lbs. impact cart on an elevated steel track, allowing it to roll down the track with a changing height of 7.8 ft. Results show that T-beam girders exhibit higher peak impact force than isolated beams, indicating better impact resistance. Moreover, the lateral displacement in the T-beam at the impact location decreased significantly by 82% compared to the isolated beam. However, failure patterns differ; prestressed beams typically experience shear failure, while conventional beams tend to fail in flexure. This research, therefore, contributes to improving the safety and resilience of bridge structures in real-world applications, design, and maintenance practices.

17. Key Words Prestressed concrete girders, Bridge safety, Lateral impact loads, Isolated and T-shaped beam, over-height vehicle collision	18. Distribution Statement

19. Security Classif. (of this report) Unclassified	20. Security Classif. (of this page) Unclassified	21. No. of Pages 25	22. Price

Table of Contents

List of Figures

List of Tables

Acknowledgements

This experimental research project was conducted in the High-bay structural laboratory of Missouri University of Science and Technology. It was funded by the Mid-America Transportation Center (MATC) and the Missouri Department of Transportation (MoDOT).

Disclaimer

The contents of this report reflect the views of the authors, who are responsible for the facts and the accuracy of the information presented herein. This document is disseminated in the interest of information exchange. The report is funded, partially or entirely, by a grant from the U.S. Department of Transportation's University Transportation Centers Program. However, the U.S. Government assumes no liability for the contents or use thereof.

Author Contributions

The authors confirm their contributions to the paper as follows: study conception and design of the experiment: M. ElGawady; data collection, analysis, interpretation of results, and draft manuscript preparation: F. Ashun, M. Abdulazeez; editing and reviewing the manuscript: M. Abdulazeez, M. ElGawady. All authors reviewed the results and approved the final version of the manuscript.

Abstract

In recent decades, there has been an increase in catastrophic vehicle-bridge collisions worldwide due to rapid infrastructure development and increased traffic. This study, which addresses the critical research gap in understanding lateral impact loads on prestressed flanged concrete bridge girders, has the potential to impact the field significantly. The paper experimentally investigates the effect of concrete decks as a restraining condition on two small-scale (20 ft long) prestressed girders: Isolated and T-shaped. Using a controlled impact load setup, these girders were subjected to lateral impacts with varying bending and torsional constraints. The test facility simulated over-height vehicle collisions using a 660 lbs. impact cart on an elevated steel track, allowing it to roll down the track with a changing height of 7.8 ft. Results show that T-beam girders exhibit higher peak impact force than isolated beams, indicating better impact resistance. Moreover, the lateral displacement in the T-beam at the impact location decreased significantly by 82% compared to the isolated beam. However, failure patterns differ; prestressed beams typically experience shear failure, while conventional beams tend to fail in flexure. This research, therefore, contributes to improving the safety and resilience of bridge structures in real-world applications, design, and maintenance practices.

Chapter 1 Literature Review

Due to the rapid development of bridge structures, transportation infrastructures, and increased traffic volume, more catastrophic vehicle-bridge collision accidents to bridge elements have been reported worldwide in recent decades. Prestressed concrete girders are commonly used in bridge construction due to their high strength-to-weight ratio, durability, and cost-effectiveness. However, when subjected to the extreme forces generated by over-height vehicle collisions, they can experience significant damage.

Such vehicle-girder collision accidents can result in severe damage to bridge superstructures, in some cases leading to the overall collapse of the substructure, as well as having strong detrimental economic shocks, increase risks to public safety, and cause loss of human life. Bridge superstructures are often struck by oversized vehicles, resulting in frequent unintended collisions globally [1-3]. In the United States, bridges are frequently struck by vehicles exceeding height limits. The state of New York experiences roughly 200 bridge collision incidents each year [2]. Therefore, studying the dynamic responses and damage and failure of bridge structures subjected to vehicular collisions is critical.

Recent devastating structural failures have prompted a reassessment of numerous prestressed concrete bridges. According to the Federal Highway Administration, impacts from vehicles or vessels are the third leading cause of bridge failures or collapses [2]. Consequently, some structures have had weight restrictions imposed, while in severe instances, bridges have been urgently taken out of service [3].

Several departments of transportation (DOTs) across the United States have reported numerous cases of bridge girders being struck by over-height vehicles, resulting in a range of damage, from minor concrete cracking to severe girder distortion, prestressing strand rupture, and even complete collapse [3]. Generally, the exterior girders that face the traffic sustain severe

damage from the collisions [3]. In most over-height collisions with bridge girders, the bottom flange and web of the girder suffers severe damage.

The impact of vehicle loads, especially when considering overloading and the dynamic effects of moving vehicles, can significantly increase the principal tensile stress in the edge beams, leading to a higher risk of diagonal cracking. The width of diagonal cracks can be used as an indicator to quickly assess the shear stiffness loss, providing a practical method for engineers to evaluate the structural health of prestressed concrete beams without complex calculations [4]. Additionally, the shear stiffness of concrete beams degrades rapidly after the first diagonal crack, with the remaining shear stiffness dropping to about 10% of the original once the stirrups yield, highlighting the importance of adequate shear reinforcement to control stiffness degradation [5]. Therefore, understanding the interplay between lateral impact loads and the resulting shear stiffness degradation is crucial for accurately assessing and designing prestressed bridge girders to prevent shear diagonal cracks and ensure long-term structural performance.

Elshazli et al. (2024) [7] conducted a numerical study focusing on the comprehensive numerical modeling of prestressed girder bridges subjected to low-velocity impacts. This is a critical study area given the potential for significant structural damage from such events. This research aligns with the findings of Yuan Jing et al. [8], who investigated the damage mechanisms of prestressed concrete (PC) box girder bridges under over-height vehicle impacts using finite element analysis, highlighting the importance of vehicle-related parameters on impact force and local damage. They underscore the importance of performing experimental studies to expand and validate their findings.

The lack of experimental studies on the lateral impact of flanged (T-Beam) prestressed concrete beam bridges is a significant gap in current research, as highlighted by various studies

on related topics. For instance, while Atul K. Senthil's research focuses on the dynamic behavior of prestressed concrete beams under impact loads, it primarily addresses vertical impacts. It does not delve into lateral impacts on flanged T-beams [10]. Similarly, the study by Airong Chen et al. [11] investigates the lateral impact loading on reinforced concrete bridge columns, revealing the importance of understanding dynamic strain and deformation under such conditions. Still, it does not extend this analysis to flanged T prestressed beams. Ahmed A. Hassan and colleagues [12] explore the behavior of reinforced HSC T-sections with flange openings under bending loads, noting the complexity introduced by such openings. Yet, they do not consider lateral impact scenarios [6]. Jinquan Zhang et al. [13] discuss the long-term performance and deflection issues in long-span concrete bridges, emphasizing the need for accurate creep and deflection predictions, but their work is more focused on vertical loads and long-term effects rather than lateral impacts.

Only one experimental test was conducted on a full-scale AASHTO type-I prestressed girder subjected to lateral impact load (Jing et al., 2016). The tested girder measured 56 feet (17.07 meters) in length and was pre-tested in shear from both ends.

That reduced the testing span for impact to 36.5 feet (11.13 meters) in the middle and two overhangs. The girder was subjected to an impact weight of 9000 lb (4082 kg) with a speed of 22.5 feet/sec (6.86 meters/sec). Only gravity and lateral supports were provided to restrain the girder. The girder was free to rotate at both ends and was allowed to uplift. The study provided only data on the girder's concrete strain and vertical displacement. The tested girder experienced punching shear failure due to the impactor's high rigidity. This is similar to the failure mode observed when testing reinforced concrete (RC) beams under impact, as discussed later in this section. An impact force of 1039 kips was deduced using a finite element model.

Most experimental testing investigations into impact behavior have focused on non-prestressed reinforced concrete (RC). The test beam had rectangular cross-sections spanning 4.6 ft (1.4 m) to 19.7 ft (6.0 m) and was tested using either drop-weight impacts (Kishi et al., 2002, 2006; Fujikake et al., 2009; Saatci & Vecchio, 2009; Zhan et al., 2015; Pham & Hao, 2017a, 2018; Pham et al., 2018; Li et al., 2019; W. Zhao et al., 2019; Fu et al., 2020) or by pendulum, as studied by (Xu et al., 2012) with the T-section. Impact weights ranged from 330 lb (150 kg) to 3740 lb (1700 kg), with impact velocities ranging from 3.3 ft/s (1.00 m/s) to 49.8 ft/s (15.20 m/s). These impact tests yielded peak impact forces within the range of 14.6 kips (65 kN) to 507 kips (2258 kN). Shear failure was the predominant failure mode manifested as a shear plug—a cone-shaped formation resulting from excessive shear forces at the impact point, leading to the outward displacement of concrete from the impacted location. Shear failure occurs due to the high shear demand resulting from the force equilibrium of the impact force and inertia forces at the impact vicinity for a very short time. At the same time, flexural failure requires relatively more time to deflect the beam, such as in static and quasi-static loading.

The American Association of Highway and Transportation Officials (AASHTO LRFD 2012) has not yet established a design force for vehicular collisions for bridge girders. The AASHTO provides a benchmark for bridge piers or abutments under impact load, defining an equivalent static force of 600 kips (2670 kN). Conversely, the Eurocode (EN 1991-2006) code outlines maximum equivalent static force values of 112 kips (500 kN) for the supporting superstructure and 224 kips (1000 kN) for the substructure.

Lastly, Rafa'a Mahmood Abbas and Wesal A. Fadala's study on the flexural behavior of reinforced concrete flanged sections underlines the impact of reinforcement distribution on flexural strength and deflection. However, it does not address lateral impact forces. Collectively,

these studies underscore the necessity for dedicated experimental research on the lateral impact resistance of prestressed concrete T-beam bridges to enhance design guidelines and ensure structural safety under such loading conditions.

Chapter 2 Experimental Work

2.1 Test Specimen Geometry and Preparation

This study examined two specimens with identical prestressing strand configurations and forces but differing top flange boundary conditions and cross-section. The test specimens were scaled-down versions of Missouri Department of Transportation (MoDOT) type 2 prestressed concrete girders. **Figure 2.1** illustrates the girders' cross-sections. The investigation involved two specimen configurations: an Isolated beam and a flanged girder (T-Beam).

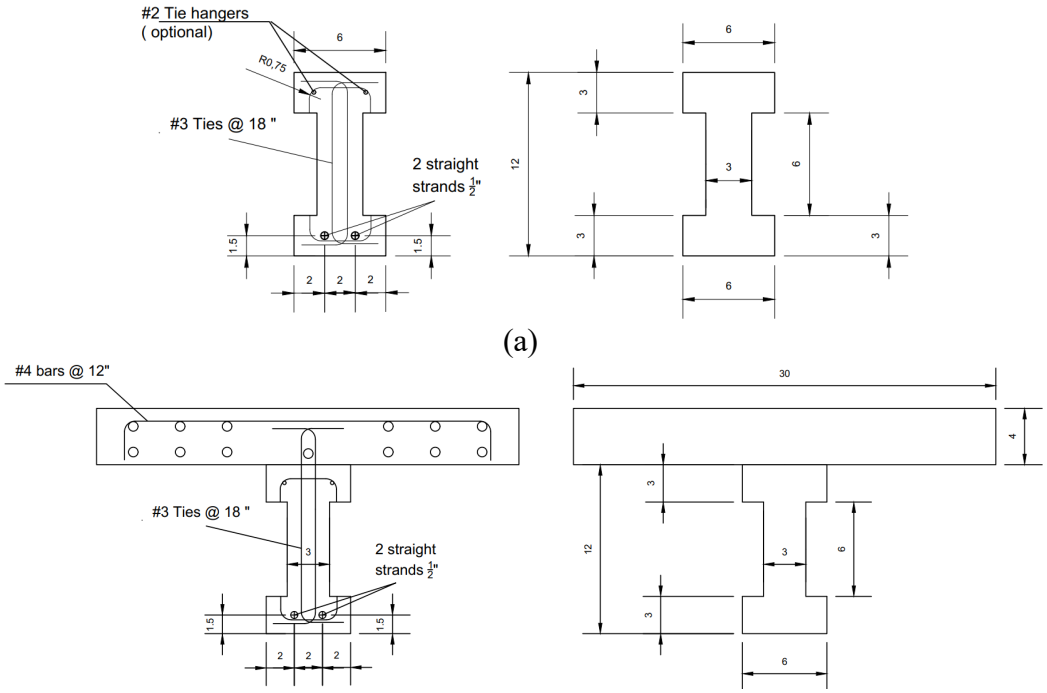

Figure 2.1 Cross section of tested specimens (a) Reinforcement details of Isolated beam, (b) Reinforcement details of T-beam

Both specimens measured 12 feet in length. The Isolated beam had a total depth of 12 inches, whereas the T-beam, including a 4-inch slab, had a total depth of 16 inches. These structural

elements were constructed in the university structural lab. Figures 2.2 a & b depict the prepared formwork and reinforcement layout for the girder before concrete casting.

2.2 Material Properties

2.2.1 Concrete

The fresh concrete mixture was placed into the prepared formwork (Figure 2.2 c & d) using mechanical vibrators for proper consolidation. Twenty-four cylindrical specimens measuring 4 x 8 inches were cast to assess the concrete's compressive strength. To prevent moisture loss, both the rafters and cylinders were covered with burlap and plastic sheets after casting. On the seventh day following casting, the prestressing strands were cut after verifying the concrete's compressive strength, and the formwork was removed (Figure 2.3 e & f). To monitor compressive strength development (f'_c), three-cylinder specimens were tested 7, 28, and 56 days after casting and on the day of girder testing. ASTM C39/C39 M conducted these testing [9] standards (Table 2.1).

Table 2.1 Concrete Properties

Days	**Average f'_c, ksi**	
	Isolated beam	**T-beam**
7	8.52	8.60
28	11.22	12.24
56	11.24	12.42
Day of Impact test	12.30	12.90

2.2.2 Prestressed strands and mild steel reinforcing bars

Each girder was prestressed with two low-relaxation, seven-wire, 0.5-in diameter steel strands.

After securing the prestressing wire in place and ensuring it is tightly anchored, the pulling jack is operated using hydraulic pressure.

(a)

(b)

(c)

(d)

(e)

(f)

Figure 2.2 Preparation of test specimens (a) Formwork and reinforcement for Isolated beam (b) Formwork and reinforcement for T-beam (c)casting of Isolated beam (d) casting of T-beam (e) Isolated beam after strand torching and demolding, and (f) T-beam demolding

The prestress force was measured using a pressure gauge on the hydraulic jack used to induce it, which was initially calibrated using a load cell (Figure 2.3). The initial prestress applied 80% of the ultimate stress of the strand for a total initial prestress force (*Pi)* = 60 kips.

a b

Figure 2.3 Strands Prestressing of test specimens (a) Isolated beam, (b) T-Beam

Table 2.2 Mechanical properties of steel reinforcement

Property	**Prestressing strand**	**Steel rebars**	
		Stirrup	***Flanges (Deck)***
Tensile strength, ksi	270	60	60
Area of steel, in^2	0.153	0.11	0.2
Nominal diameter, in	0.5	0.375	0.5

The deck was reinforced with a 0.5-in diameter mild steel bar 12 in. in the center as the main bar and six 0.5-in. diameter mild steel bars were used as temperature and shrinkage reinforcement. Stirrups with a 0.375 in. diameter at 18 in. in the center were used in the girder as

transverse reinforcement. Table 2.2 shows the mechanical properties of the prestressed strands and mild steel reinforcing bars.

2.3 Test setup and instrumentation

To simulate vehicular collision against bridge prestressed girders, an impact load was imposed using a cart that slides on a rollercoaster track. This experimental setup is illustrated in Figure 2.4 a. The experimental configuration utilized girders with simply supported boundary conditions resting on 30-inch-high steel gravity supports. The setup incorporated vertical and lateral supports to ensure stability during impact. Additionally, the girder was secured at both ends using HSS6x6x3/8" sections and 1.57-in. diameter threaded dywidag bars, creating tie-down points to the lab's strong floor to prevent overturning of the girder during impact. The rollercoaster track was manufactured using a steel tube frame with a total projection length of 229 inches and height of 94 inches and fixed firmly to the strong floor Figure 2.4 b.

The cart, weighing 365 lb. and measuring 27.5 in. x 30 in., was pulled to the apex of the 220-in. long, 94-in. high track, inclined at 59 degrees, using a 5,000-lb capacity electric winch. On top of it was an additional 295-lb, 4.5-in. thick reinforced concrete slab (Figure 2.4c). The impactor head, crucial for the specimen's response, was a 1 in. x 3 in. x 4.5 in. rectangular steel plate.

A 200-kip capacity load cell between the impactor and cart measured the impact force. To measure reaction forces, another 200-kip capacity load cell was placed between the two lateral supports and the girder.

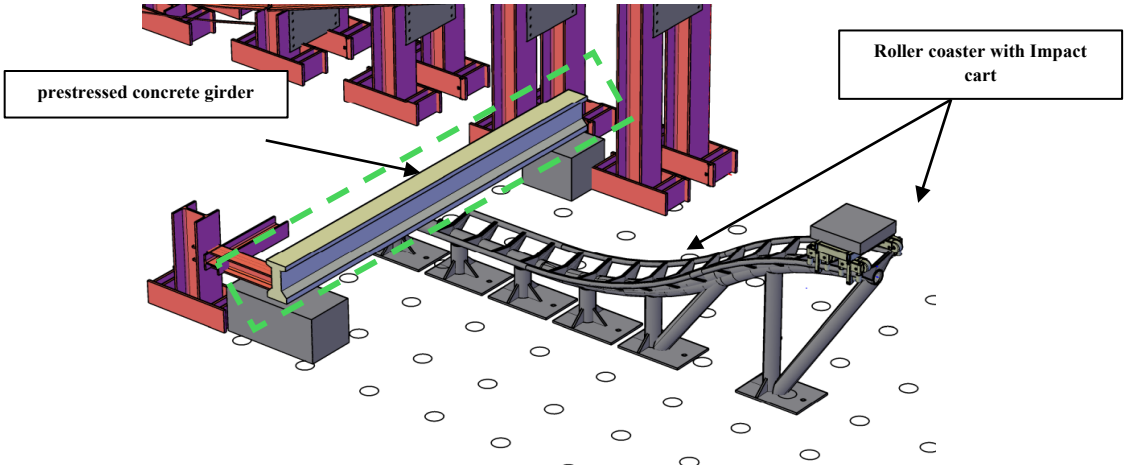

(a)

(b)

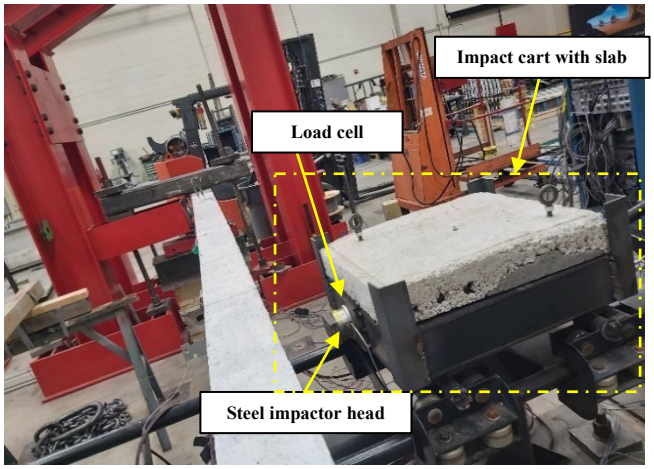

(c)

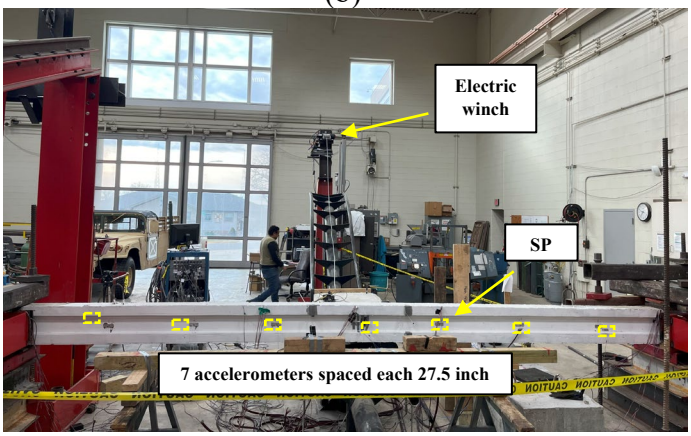

(d)

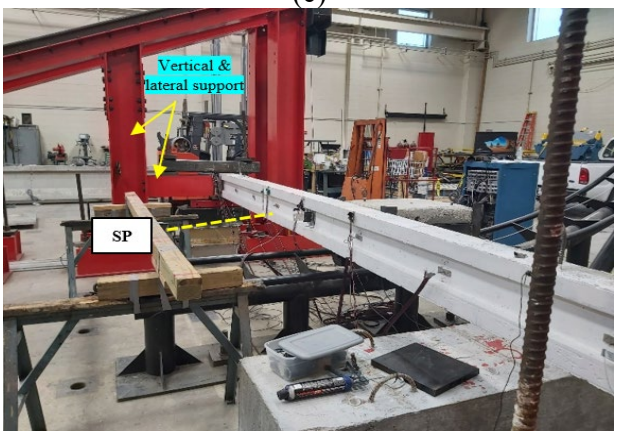

(e)

Figure 2.4 Experimental test setup (a) Schematic of overall test setup (b) Roller coaster with impact cart (c) Impact cart instrumented with load cell and front steel plate (d) accelerometer installation on girder and (e) String potentiometer (SP)

Twenty-six strain gauges were used on the steel in total, six on the strands and the remaining on the stirrups, to monitor the distribution of longitudinal and transverse strains during the impact. Seven string-potentiometers (SP) were utilized to measure displacements during the test. Five out of the seven were located around the midspan of the girder, and the remaining two were attached to the east of the girder at the top flange, one on either side of the girder (front face and rear face) to measure the rotation of the girder at the ends. One of these five SPs was located on the midspan web of the girder to measure the lateral deflection, and each two out of the four was placed on the top and bottom flange of the girder 16-in. away from the midspan to monitor the rotation of the girder around the midspan. To measure the girder's acceleration during impact, seven Kistler shock piezoelectric accelerometers having a capacity of 5000 g were positioned along the back of the girder's web. These were spaced at intervals of 27.5 inches in the longitudinal direction of the girder. A high-speed data collection system at 50,000 Hz connected all sensors and measuring equipment. This rapid sampling rate allowed for recording the quick fluctuations in impact forces and the girder's subsequent reactions.

Table 2.3 Impact Test Parameters

Beam	**Impact speed m/sec**	**Impact mass, *lbs***
Isolated	4.96	660
T	4.96	660

Chapter 3 Results and Discussions

3.1 Global behavior

The cart was released and hit the midspan of the prestressed concrete girder specimens. A visual inspection was conducted to evaluate the damage to both girders after the impact event. The average impact cart speed measured using an accelerometer mounted on the cart was 11.09 mph. The peak impact forces for Isolated and T-beams were 32 and 76 kips, respectively. The lateral displacement decreased significantly by 82%, from 7.4 inches for the isolated beam to 1.45 inches for the T-beam (Figure 3.1). The strands were exposed but not ruptured. The strand damage can be attributed to the axial tensile and compression stresses caused by the section's biaxial bending. The biaxial bending resulted from the in-plane bending due to the prestressing force that cambers the girder upward and the out-of-plane bending due to the outward deflection caused by the impact force.

Table 3.1 Impact Force Results

Beam	Impact Force, kips
Isolated	32
T	76

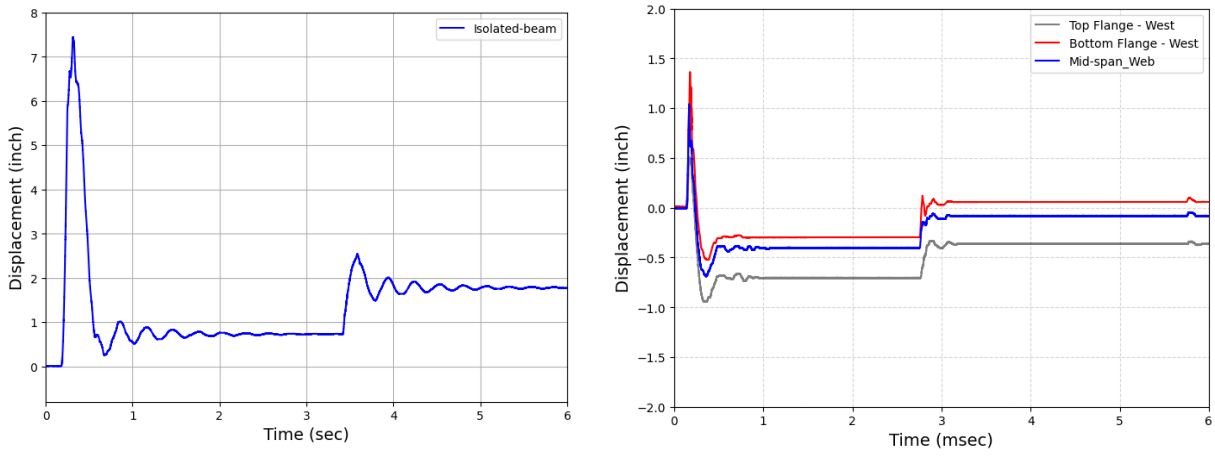

(a) (b)

Figure 3.1 Lateral displacement time history for (a) Isolated beam, and (b) T-beam

3.1.1 Isolated beam

The impact caused localized scabbling and spalling of concrete at the impact point on the girder's bottom flange and web, as well as on the top flange (Figure 3.2 a) due to compressive stress waves, resulting in the loss of approximately 48% of the concrete cross-section. Additional spalling occurred on the opposite side's top flanges due to tensile waves caused by concrete crushing from contact energy. With the continuation of the impact process, the concrete in the web transition, top flange, and bottom flange undergo significant plastic deformation, multiple cracks appear, and the concrete on the impact side begins to spill. Due to the influence of bending and shear, there was also noticeable plastic deformation at the interface of the web and the top flange on the other side of the beam (Figure 3.2 b, c, d & e).

The concrete in the midspan area of the impact beam is crushed and falls. The impact leads to the beam's bending failure and the formation of numerous parallel shear cracks along the beam. The concrete spalling was caused by crushing the concrete at the impact location due to the contact energy, which caused the penetration of the impactor head. Also, the excessive deflection of the girder during the impact load led to the spalling of the bottom flange at the back and top flange. The maximum lateral displacement reached was 7.4 in. with 1.125 in. residual displacement, corresponding to 0.47% lateral residual drift (Figure 3.1 a).

Shear cracks developed along the length of the girder, with crack widths ranging from 0.004-inch diagonal hairline cracks to a 0.1-inch vertical crack at the tensile face of the impact point (Figure 3.2 d). The failure of the specimen is first introduced by punching shear around the impact zone due to the relatively high rigidity of the impactor, as well as the high compressive strength of the PC girder. This phenomenon can also be observed from girder backside diagonal and horizontal cracks between the web and bottom flange. With the penetration of the impactor,

the damaged impact zone behaves as a ‘hinge’ that moves upward and laterally due to the compressive prestressing forces and the severity of the impact event. A visual inspection after testing showed that none of the prestressing strands had become unbundled (Figure 3.2 c) despite the damage.

3.1.2 T-beam

The T-beam specimen underwent a lateral impact loading scenario like the isolated beam at the same speed but with partial restraint provided by a cast-in-place reinforced concrete deck acting on the top flange. This deck partially restrained horizontal and vertical translation of the top flange during impact. The cracking pattern that developed along the length of the T-beam was mainly around the impact region, 48 in. away from the supports (Figure 3.3 a and b), with closer crack spacing compared to the Isolated beam test at the same impact energy level. The concrete in the impact area is crushed, and cracks appear, with some steel bars yielding. Furthermore, the concrete on the other side of the beam sustains relatively plastic damage

Shear cracks dominated the girder's span, propagating from the bottom flange to the junction of the web and the top flange. Additionally, vertical cracks propagated in the front face of the deck and up into the concrete deck slab itself. This contrasted with the Isolated beam, which exhibited a more flexible response. Unlike the more flexible Isolated beam, the T-beam exhibited a stiffer response due to the top flange restraint. This increased stiffness led to extensive concrete scabbling and spalling of the bottom flange (Figure 3.3 c), particularly on the girder's tensile face and soffit (Figure 3.3 d & e), resulting in the loss of approximately 56% of the concrete cross-section. Interestingly, the top flange was almost intact due to the presence of the concrete deck restraining in Figure 3.3 c.

(a)

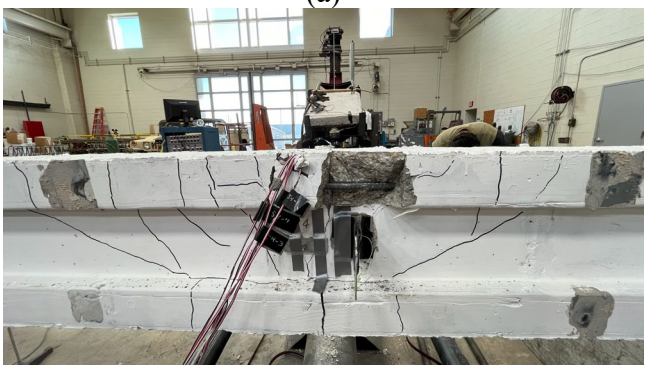

(b)

(c)

Figure 3.2 Characteristic damage pattern after impact – Isolated beam (a) Crack propagation and spalling of concrete – front view (b) Concrete deterioration and fissure development – rear view (e) Top view of concrete degradation and crack formation

Cracks ranged from 0.005 in. up to 0.02 in. within the concrete deck, illustrated in Figure 3.3 f, due to the upward bending of the prestressed T-beam during the impact event, while diagonal crack widths within the girder ranged from 0.005 in. to 0.1 in. A horizontal crack shown in Figure 3.3 d greater than 0.1 in. was induced within the girder at the transition of the bottom flange and the web, attributed to the added stiffness from the flange restraint. At midspan, the maximum

lateral displacement was 1.4 in., with no residual displacement, which can be attributed to the effect of the concrete deck restraining by providing more sectional stiffness (Figure 3.3 b).

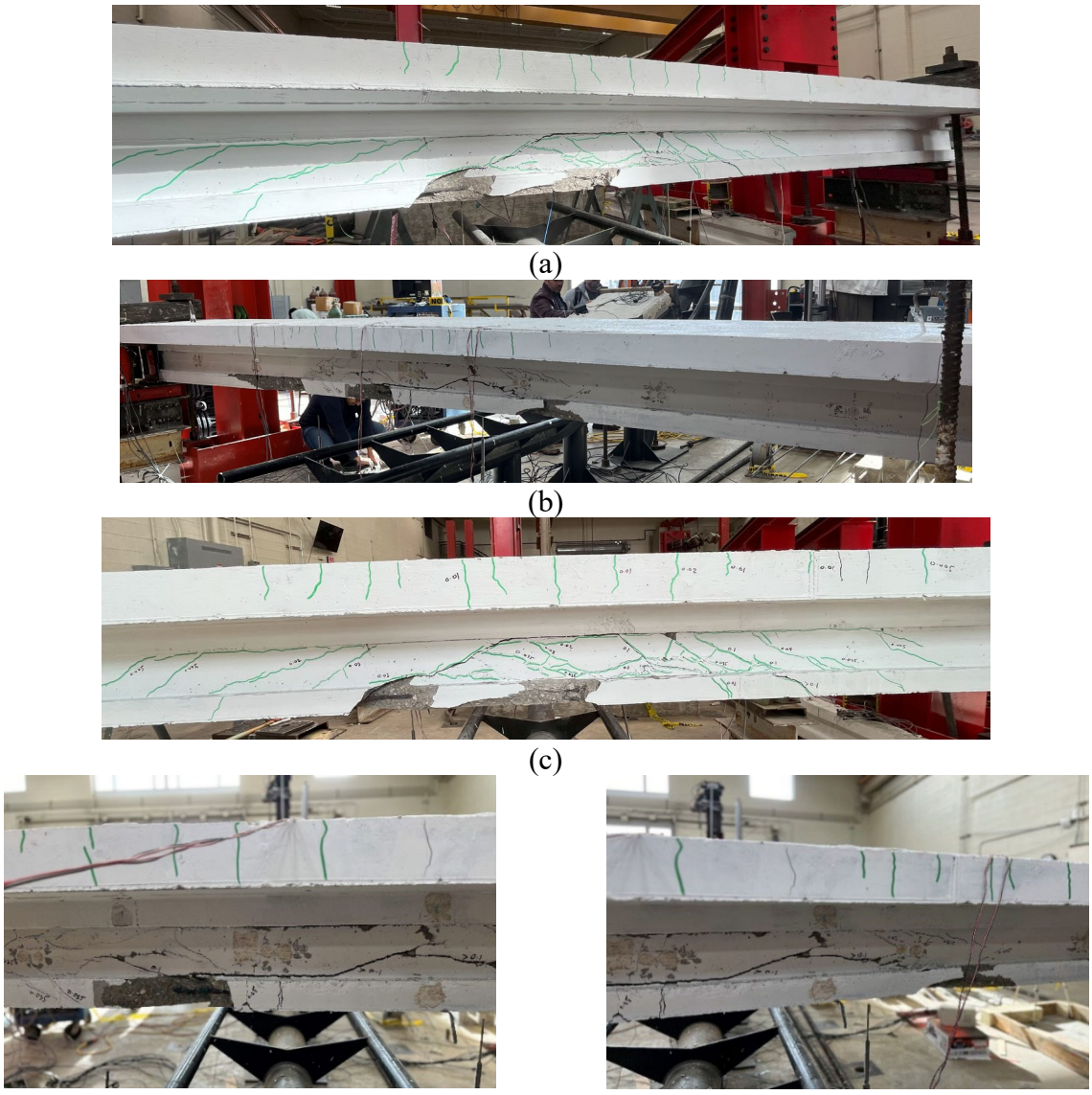

Figure 3.3 Characteristic damage pattern after impact – T-beam (a) Crack propagation and spalling of concrete – front global view (b) Concrete deterioration and fissure development – rear global view (c) Front view of local damage and strand exposure (d) Rear view of local damage (e) Close-up view of a concrete girder showing significant spalling and cracking along its underside, highlighting structural damage, and (f) Top view of crack formation within deck

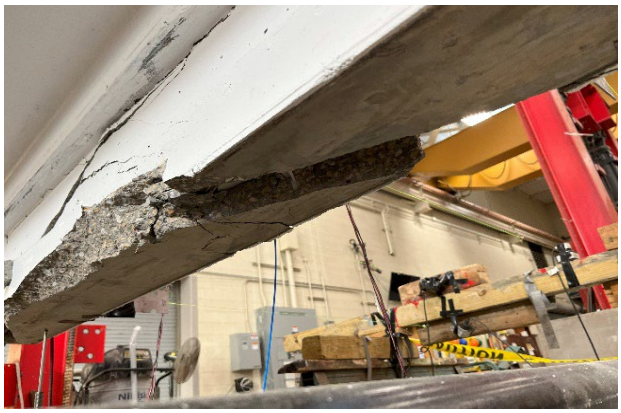

(e)

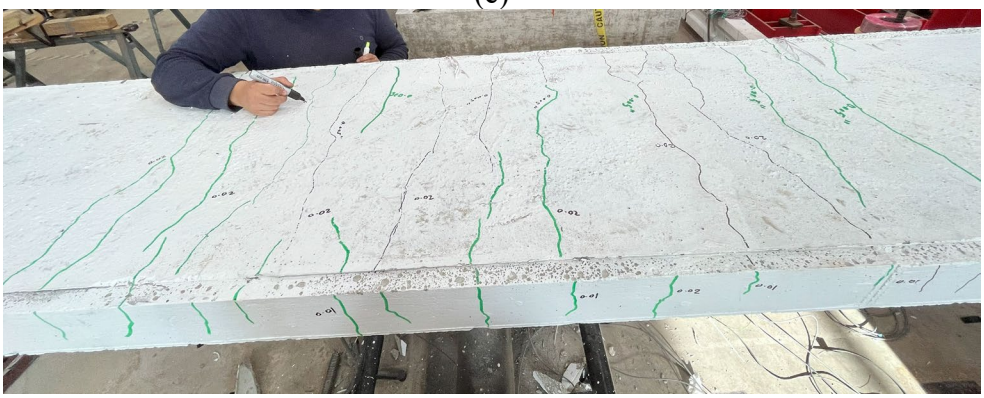

(f)

Figure 3.3 cont. Characteristic damage pattern after impact – T-beam (a) Crack propagation and spalling of concrete – front global view (b) Concrete deterioration and fissure development – rear global view (c) Front view of local damage and strand exposure (d) Rear view of local damage (e) Close-up view of a concrete girder showing significant spalling and cracking along its underside, highlighting structural damage, and (f) Top view of crack formation within deck

3.2 Impact Forces

Figure 3.4 displays the time history of impact forces for girders 1 and 2. The data acquisition system captured the time history of the impact force for each test. During the first 2.5 milliseconds of impact, the force pattern showed a sharp triangular peak as contact was made. This was followed by free vibration that decayed over 22.5 milliseconds of the total 25-millisecond impact duration. The peak force depended on several factors: impact speed, mass, local contact stiffness, and overall girder stiffness. The beam system's global stiffness primarily determined the subsequent free vibration phase. For the isolated beam, the peak force was 32 kips (Figure 3.4 a),

whereas it increased to 76 kips (Figure 3.4 b) for the T-beam, which is more than 50% of the force. This higher impact force increased the acceleration of the T-beam specimen, aligning with conservation of momentum principles based on the velocity generated in the beam by the impact cart's collision.

For the impacted isolated beam (Figure 3.4 a), at the instant of contact between the impactor head and the concrete beam, the impact force increased almost linearly with time, which indicates that concrete deformed in its elastic range and severe local punching failure was observed in the isolated beam at the impact area. At t = 0.2 ms, the slope of the impact force-time curve started to reduce since the specimen's stiffness decreased due to local deformation. At t = 0.9 ms, the impact force reached its maximum value of 33 kip. The impact force dropped dramatically after that to almost zero. At t = 5 ms, the impact force increased again to 14 kips because the speed of the girder tended to be smaller than that of the impact cart, and the contact area between the impactor and the girder became larger. After that, a small vibration was introduced to the girder, resulting in a large fluctuation of the curve as the dynamic responses mainly depend on the local stiffness rather than the overall stiffness along the impact direction. At about t = 10 ms, the impact force tended to be stable. The area under the impact force-time curve revealed small impact energy was absorbed as the impacted I-beam was severely damaged. Figure 8A shows that the impacted beam reached 7.4 inches with noticeable residual displacement due to the permanent impact damage.

For the impacted T-beam (Figure 3.4 b), at the instant of contact between the impactor head and the concrete beam, the impact force increased almost linearly with time, which indicates that concrete deformed in its elastic range. At t = 0.3 ms, the slope of the impact force-time curve started to reduce since the specimen's stiffness decreaseed due to local deformation. At t = 0.7 ms,

the impact force reached its maximum value of 76 kip. The impact force dropped dramatically after that because the speed of the specimen moving forward was larger than that of the impact cart, and the girder was trying to separate from the impact. At t = 3.5 ms, the impact force increased again to 33 kips because the speed of the girder tended to be smaller than that of the impact cart, and the contact area between the impactor and the girder became larger. After that, the impact force decreased due to local deformation and the probability of a smaller contact area when the girder moved upward. At the same time of 7 ms, a small vibration was introduced in the girder, resulting in a small fluctuation of the curve, and at about t = 10 ms, the impact force tended to be more stable due to the presence of the concrete deck restraining. compared to the Isolated, tested beam. The area under the impact force-time curve revealed large impact energy was absorbed as the impacted T-beam sustained the primary energy.

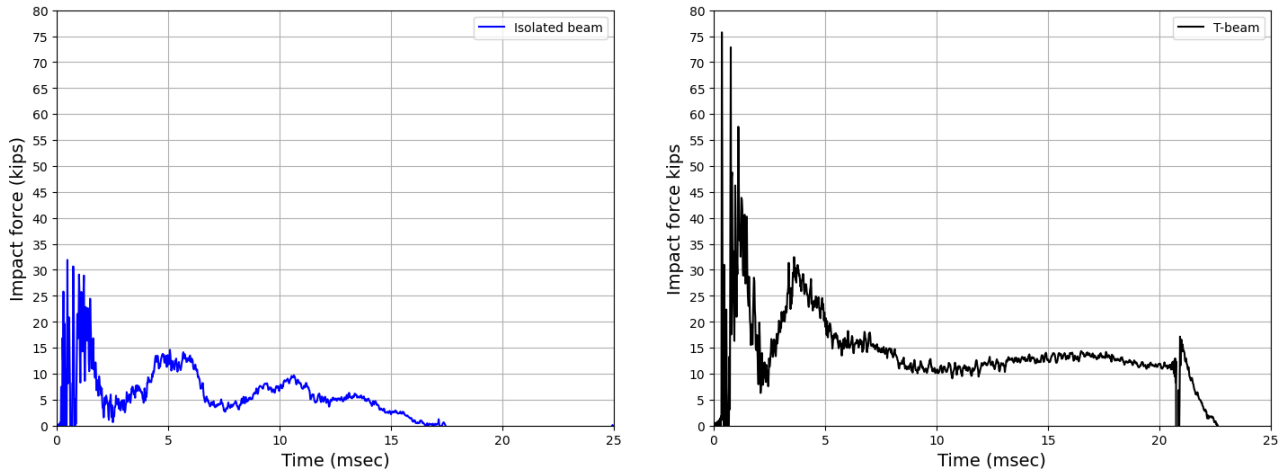

(a) (b)

Figure 3.4 Impact forces time histories for (a) Isolated beam, and (b) T-beam

Figure 3.5 depicts the time histories of support reaction forces. The peak east support reactions measured 13 and 40 kips for Isolated and T beams, respectively. The relatively low

value of peak support reactions compared to the peak impact forces can be attributed to the inertial forces that immediately responded to the impact event.

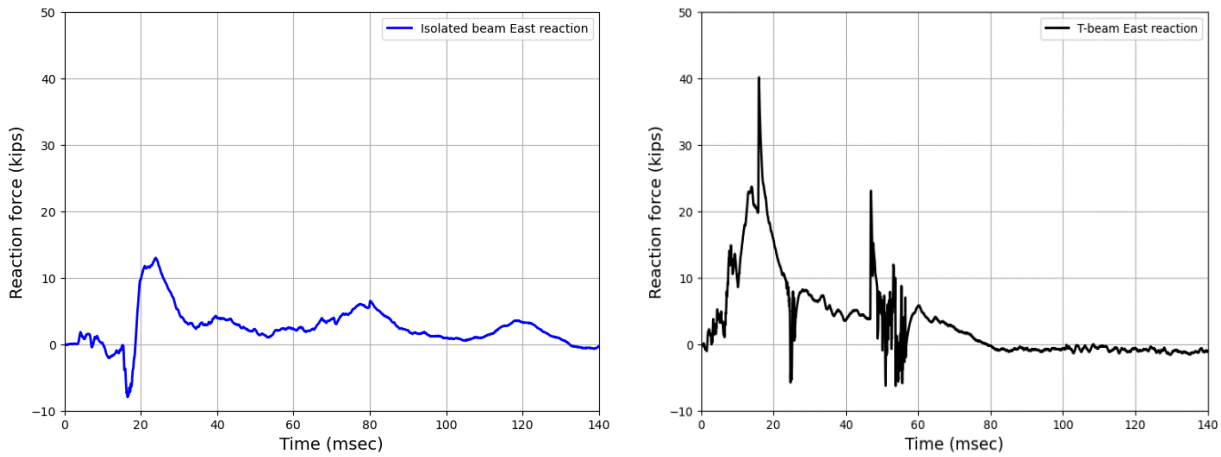

(a) (b)

Figure 3.5 Time histories of support reaction forces (a) Isolated beam, and (b) T-beam

Chapter 4 Conclusions

This report aims to investigate experimentally the effect of the concrete deck on impact testing of two small-scale (20 ft long) prestressed girders, Isolated I and T-shaped. These girders were subjected to lateral impact loads with different bending and torsional constraints using a controlled impact load setup. The lateral impact testing facility can recreate the impact damage by an over-height vehicle collision. This was accomplished by impacting a test specimen of 660 lb. with an impact cart. The impact cart was raised on an elevated steel track and allowed to roll down the track with a changing height of 7.8 ft.

The results reveal that prestressed concrete beams, such as T-beam girders, exhibit a higher peak impact force than Isolated beams, indicating better resistance to impact loads. However, the failure patterns differ, with prestressed beams typically experiencing shear failure under impact loads, while conventional beams tend to fail mainly flexural. These findings, providing a comprehensive understanding that can inform design and maintenance practices, suggest that while both T-shaped and I-shaped girders can be effectively used in bridge construction, their performance under lateral impact loads can be optimized through appropriate prestressing and shear strengthening techniques.

References

1. L. J. Xu, X. Z. Lu, S. T. Smith, and S. T. He, “Scaled model test for collision between over-height truck and bridge superstructure,” *Int J Impact Eng*, vol. 49, pp. 31–42, 2012, doi: 10.1016/j.ijimpeng.2012.05.003.

2. Agrawal, Anil K., Xiaochen Xu, and Zheng Chen. *Bridge-vehicle impact assessment*. No. C-07-10. University Transportation Research Center, 2011.

3. Harries, Kent A. "Structural testing of prestressed concrete girders from the Lake View Drive Bridge." *Journal of Bridge Engineering* 14, no. 2 (2009): 78-92.

4. Oppong, K., Saini, D., & Shafei, B. (2021a). Characterization of impact-induced forces and damage to bridge superstructures due to over-height collision. Engineering Structures, 236, 112014. https://doi.org/10.1016/j.engstruct.2021.112014

5. Oppong, K., Saini, D., & Shafei, B. (2021b). Ultrahigh-performance concrete for Improving Impact Resistance of Bridge Superstructures to Overheight Collision. Journal of Bridge Engineering, 26(9), 04021060. https://doi.org/10.1061/(asce)be.1943-5592.0001736

6. Kunning, Zhu. Research on Diagonal Cracks in the Mid Span of Prestressed Concrete Composite Box Girder Bridge. Advances in transdisciplinary engineering, (2023). doi: 10.3233/atde230817

7. Kaiqi, Zheng., Yaohui, Zhang., Yang, Wei., Jia-Qing, Wang., Xiaochuan, Qin. Simplified Evaluation of Shear Stiffness Degradation of Diagonally Cracked Reinforced Concrete Beams. Materials, (2023). doi: 10.3390/ma16134752

8. Jinliang, Liu., Yanmin, Jia., Guanhua, Zhang., Jiawei, Wang. Effect of diagonal cracks on shear stiffness of pre-stressed concrete beam. International Journal of Structural Integrity, (2018). doi: 10.1108/IJSI-07-2017-0042

9. Elshazli, Mohamed T., Mohanad M. Abdulazeez, Mohamed ElGawady, and Ahmed Ibrahim. "Comprehensive Numerical Modeling of Prestressed Girder Bridges under Low-Velocity Impact." *Buildings* 14, no. 3 (2024): 640.

10. Yuan, Jing., Yu, Zhen, Zhao., Yongjun, Zhou. Damage mechanism and damage evaluation of PC box girder bridge subjected to overheight vehicle impact. Structural Concrete, (2023). doi: 10.1002/suco.202201049

11. American Society for Testing and Materials. Committee C09 on Concrete and Concrete Aggregates. *Standard test method for compressive strength of cylindrical concrete specimens*. ASTM International, 2021.

12. Atul., K., Senthil. (2024). Response of prestressed reinforced concrete beam under impact loading through the experiment. IOP conference series, doi: 10.1088/1755-1315/1326/1/012031

13. Airong, Chen., Yanjie, Liu., Rujin, Ma., Xiaoyu, Zhou. (2023). Experimental and Numerical Analysis of Reinforced Concrete Columns under Lateral Impact Loading. Buildings, doi: 10.3390/buildings13030708

14. Ahmed, A., Hassan., Fouad, Khairallah., Hala, Mamdouh., Aya, Allah, Gamal, Ahmed, Mahmoud. (2022). Experimental Study of High Strength Concrete T-Sections with Flange Openings. International Journal of Advances in Structural and Geotechnical Engineering, doi: 10.21608/asge.2022.274730

15. Jinquan, Zhang., Ping, Fan., Shou-shan, Cheng. (2023). Experimental Study on Long-Term Performance of Concrete T-Beam. Buildings, doi: 10.3390/buildings13041005

16. Miele, C. R., Plaxico, C., Stephens, D., & Simunovic, S. (2010). U26: Enhanced Finite Element Analysis Crash Model of Tractor-Trailers (Phase C). Phase C, 276p.

17. O'toole, B., K. Karpanan, and M. Feghhi. *Experimental and finite element analysis of preloaded bolted joints under impact loading*. in *47th AIAA/ASME/ASCE/AHS/ASC Structures, Structural Dynamics, and Materials Conference 14th AIAA/ASME/AHS Adaptive Structures Conference 7th*. 2006.

18. Hadjioannou, M., D. Stevens, and M. Barsotti. *Development and validation of bolted connection modeling in LS-DYNA® for large vehicle models*. in *14th International LS-DYNA Users Conference*. 2016.

19. Thai, Huu-Tai, Vo, Thuc, Nguyen, Trung-Kien and Pham, Cao Hung (2017) Explicit simulation of bolted endplate composite beam-to-CFST column connections. Thin-Walled Structures, 119. pp. 749-759. ISSN 0263-8231

20. Wu Y, Crawford JE. Numerical Modeling of Concrete Using a Partially Associative Plasticity Model. J Eng Mech. 2015;141(12):04015051.

21. Chehab, A. I., Eamon, C. D., Parra-Montesinos, G. J., & Dam, T. X. (2018). Shear testing and modeling of AASHTO type II prestressed concrete bridge girders. ACI Structural Journal, 115(3), 801–812. https://doi.org/10.14359/51701917

22. Olsen, S. A. (1992). Reusability and Impact Damage Repair of Twenty-Year-Old AASHTO Type III girders.

23. Ludovico. (2005). Repair of Bridge Girders with Composites: Experimental and Analytical Validation. ACI Structural Journal, 102(5). https://doi.org/10.14359/14659

24. Guo, J., Cai, J., & Chen, W. (2017). Inertial Effect on RC Beam Subjected to Impact Loads. International Journal of Structural Stability and Dynamics, 17(4), 1–23. https://doi.org/10.1142/S0219455417500535

25. Li, H., Chen, W., & Hao, H. (2020). Factors influencing impact force profile and measurement accuracy in drop weight impact tests. International Journal of Impact Engineering, 145(February 2021). https://doi.org/10.1016/j.ijimpeng.2020.103688

26. Pham, T. M., & Hao, H. (2017). Effect of the plastic hinge and boundary conditions on the impact behavior of reinforced concrete beams. International Journal of Impact Engineering, 102, 74–85. https://doi.org/10.1016/j.ijimpeng.2016.12.005

27. Zhao, Weiguo, Liying Wang, and Zhenxing Zhang. "Atom search optimization and its application to solve a hydrogeologic parameter estimation problem." *Knowledge-Based Systems* 163 (2019): 283-304.